Applied Catalysis B: Environmental 96 (2010) 117–125

Contents lists available at ScienceDirect

Applied Catalysis B: Environmental

journal homepage: www.elsevier.com/locate/apcatb

Total oxidation of propene over Au/xCeO$_2$-Al$_2$O$_3$ catalysts: Influence of the CeO$_2$ loading and the activation treatment

Pandian Lakshmanan, Laurent Delannoy, Vincent Richard, Christophe Méthivier, Claude Potvin, Catherine Louis *

Laboratoire de Réactivité de Surface, UMR 7197 CNRS, Université Pierre et Marie Curie-UMPC, 4 place Jussieu, 75252 Paris Cedex 05, France

ARTICLE INFO

Article history:
Received 24 November 2009
Received in revised form 28 January 2010
Accepted 4 February 2010
Available online 11 February 2010

Keywords:
Au/CeO$_2$
Au/Al$_2$O$_3$
Au/CeO$_2$-Al$_2$O$_3$
Gold catalyst
VOC oxidation
Propene oxidation
EFTEM
XPS

ABSTRACT

This study explores the reaction of oxidation of propene (1200 ppm) under excess oxygen (9%) over Au/xCeO$_2$/Al$_2$O$_3$ catalysts (x = 1.5, 3, 5, and 10 wt% CeO$_2$) to mimic the conditions of VOC decomposition. The present study reveals the influence of several factors that affect the oxidative performance of the Au/xCeO$_2$/Al$_2$O$_3$ catalysts, such as the ceria loading, the catalyst activation method, i.e., the gold oxidation state, the gold particle size and the distribution of gold on ceria and alumina. The Au/xCeO$_2$/Al$_2$O$_3$ catalysts were found 100% selective to CO$_2$. Their activity was intermediate between that of Au/Al$_2$O$_3$ (poorly active) and Au/CeO$_2$ (active). Interestingly, the activity increased with the ceria loading when the samples were activated under H$_2$ at 300 °C, but decreased when they were activated under O$_2$ at 500 °C. Characterization of the Au/xCeO$_2$/Al$_2$O$_3$ catalysts after both types of activation was performed by TEM, EFTEM, XPS and CO oxidation reaction. The results show that whatever the mode of activation, as the CeO$_2$ loading increased, the proportion of gold particles on alumina decreased while that on ceria increased, but gold remained unreduced on ceria after calcination under O$_2$ whereas it was metallic after reduction under H$_2$. Gold on ceria being more active when it is metallic than when it is unreduced, this explained the evolution of the catalytic results of propene oxidation as the ceria loading varied.

1. Introduction

Gold supported on ceria has been reported to be effective for total oxidation of CO and of a variety of other molecules, [1] such as methanol, iso-propanol, toluene [2], benzene, chlorobenzene, hexane [3] propene [4] and formaldehyde [5]. For propene oxidation and also for iso-propanol [6], benzene [3,7], chlorobenzene and hexane oxidation [3], gold on ceria is more effective than ceria alone [2,3] or than gold supported on other supports such as Al$_2$O$_3$, TiO$_2$, and ZrO$_2$ [3,4,8]. In addition to the gold particle size and the conditions of catalyst activation [8,9], the CeO$_2$ preparation method, its surface area, particle size and nature of the exposed crystal planes are also known to influence the catalytic performance of gold supported on ceria for CO oxidation [10,11] and water-gas shift [12,13]. However, CeO$_2$ is not considered as a suitable support for catalytic applications due to poor thermal stability against sintering and loss of its unique oxygen storage/release properties. To overcome these drawbacks, Al$_2$O$_3$ support can be used to stabilize ceria [14].

The aim of the paper is to study the performances (activity, selectivity and stability) of Au/CeO$_2$-Al$_2$O$_3$ catalysts with various ceria loadings in the total oxidation of propene, and to compare them to those of Au/CeO$_2$ and Au/Al$_2$O$_3$ systems. Moreover, the paper also focuses on how the interactions between gold and ceria vary with the ceria loading and affect the catalytic activity. Indeed, ceria can be present on alumina as three-dimensional particles (3D-CeO$_2$ at high ceria loading, above the monolayer coverage) and two-dimensional ceria layers (2D-CeO$_2$, below the monolayer coverage); both of these differ from unsupported CeO$_2$, with respect to the oxidation state of cerium [15,16]. For instance, CeO$_2$ in CeO$_2$-Al$_2$O$_3$ samples containing low Ce loadings and highly dispersed ceria was found more reducible than 3D-CeO$_2$ particles at higher loadings and than unsupported CeO$_2$ [15,16].

The CeO$_2$-Al$_2$O$_3$ supports are generally prepared by impregnation of alumina with cerium nitrate solutions [4,16–18] or by mechanical mixing of alumina and cerium hydroxides [19], with ceria loadings varying within a broad range, from 1 to 40 wt%. In the few studies on gold catalysts supported on CeO$_2$-Al$_2$O$_3$ supports, the ceria loadings are limited to high amounts, 10 to 20 wt% [4,18,19]. In the present investigation, ceria was deposited by impregnation and the amount of ceria was systematically varied from 1.5, 3, 5, and 10 wt% CeO$_2$, i.e., in a range of loadings where ceria can exhibit different morphologies.

* Corresponding author.
E-mail address: catherine.louis@upmc.fr (C. Louis).

0926-3373/$ – see front matter © 2010 Elsevier B.V. All rights reserved.
doi:10.1016/j.apcatb.2010.02.009

1 wt% of gold was deposited on the CeO_2-Al_2O_3 supports by the method of deposition–precipitation with urea that was developed in our laboratory [20,21]. Conventional TEM cannot reveal small gold particles on ceria with high surface area [12,22], due to the poor contrast between Au and CeO_2. This is especially true when the sizes of Au and CeO_2 particles are in the same range. To overcome this problem, authors used larger ceria grains with lower surface area and low index facets [12,23,24]. In the present study, in addition to TEM, Energy Filtered Transmission Electron Microscopy (EFTEM), which is a technique of chemical contrast imaging, was performed to distinguish the different elements by elemental mapping.

Gold oxidation state in the Au/$x$$CeO_2$-$Al_2O_3$ samples was evaluated using XPS. However, we will see that gold reduces during XPS measurement even when the samples are cooled down to 100 K. As a consequence, the reaction of CO oxidation at room temperature was used as a characterization tool to provide information on the gold oxidation state. Indeed, in a former paper of ours [22], gold samples prepared with the same method of deposition–precipitation with urea, with the same supports of alumina and ceria and with the same gold loading of 1 wt%, were found active in CO oxidation when metallic gold was supported on ceria (reducible support) but inactive over gold on alumina (non-reducible support), and over calcined Au/CeO_2 as gold was not reduced during calcination at 500 °C.

2. Experimental

2.1. Catalyst preparation

CeO_2-Al_2O_3 supports containing different CeO_2 loadings (1.5, 3, 5 and 10 wt% with respect to Al_2O_3) were prepared by impregnation in excess of solution. The requisite quantity of $Ce(NO_3)_3{\cdot}6H_2O$ (Aldrich, 99.9%) was dissolved in distilled water (~25 mL). 5 g of Al_2O_3 (AluC Degussa, 110 $m^2\,g^{-1}$) was added slowly to the solution to avoid the formation of a thick paste, and then vigorously stirred for 2 h at room temperature. Gradual removal of excess water was performed with a rotary evaporator at 60 °C. The resulting powder was then oven dried at 120 °C for 2 h and finally calcined at 500 °C with a ramp of 5 °C min^{-1} from room temperature to 500 °C then 5 h at 500 °C under a flow of 9% O_2 in He (100 mL min^{-1}).

1 wt% of gold was loaded on the various CeO_2-Al_2O_3 samples by deposition–precipitation with urea (DPU), as described previously [20,21]. In a typical preparation, 2 g of calcined and finely powdered CeO_2-Al_2O_3 sample was dispersed in distilled water. The slurry temperature was fixed at 80 °C, and then a solution (300 mL, $5{\cdot}10^{-4}$ M) of commercial $HAuCl_4{\cdot}3H_2O$ (Acros, chloroauric acid) was added, followed by the addition of 3 g of urea (Prolabo, 98%). The resulting mixture was stirred for 12 h in the reactor at 80 °C, covered by opaque aluminum foil to avoid uncontrolled gold photo-reduction. The solid was gathered after centrifugation, then washed three times with distilled water and dried under vacuum at room temperature. The samples were stored at ambient temperature and under vacuum in a desiccator, away from light in order to prevent any alteration [25]. At this stage of the preparation, the gold catalysts are referred to "as prepared" samples. For the purpose of comparison, pure supports such as CeO_2 (HSA-5, Rhodia, 200 $m^2\,g^{-1}$) and Al_2O_3 (AluC Degussa, 110 $m^2\,g^{-1}$) were also used to load 1 wt% gold by the same procedure. Aliquots of samples were either activated under a flow of 9% O_2 in He at 500 °C (calcination) or under pure H_2 at 300 °C (reduction) (100 mL min^{-1}, 2 °C min^{-1} from room temperature to the final temperature then 2 h at the final temperature). Note that for the sake of brevity, these treatments are called calcination and reduction, respectively in the following, but this does not necessarily relate to the gold oxidation state in the samples.

2.2. Techniques

Chemical analyses were performed by inductively coupled plasma atom emission spectroscopy at the CNRS Centre of Chemical Analysis (Vernaison, France). The Au and CeO_2 loadings were expressed as wt%. XRD analysis was carried out with a Siemens D500 diffractometer with Cu K_α radiation.

TEM analysis was performed using a JEOL 100 CX II microscope. The size limit for gold particles detection is in principle about 1 nm. Gold particle size measurements were performed particle by particle, using ITEM software on digitized micrographs. The average metal particle sizes d_{Au} were determined from the measurement of at least 300 particles, and d_{Au} was calculated using the following formula: $d_{Au} = \Sigma n_i d_i / \Sigma n_i$ where n_i is the number of particles of diameter d_i.

Energy Filtered Transmission Electron Microscopy (EFTEM) was performed with a JEOL 2100 FEG UHR microscope with a GATAN imaging filter 2001. EFTEM permits chemical contrast imaging (Elemental Mapping) of samples with a resolution of nearly 1 nm. EFTEM is based on the inelastic scattering of electrons passing through the sample. Resulting spectra have three main features: zero-loss peak, low-loss region, and characteristic absorption edge at higher energy. Absorption edges are useful for elemental analysis since they derive from the inner shell excitation of the sample elements. The following energy edges were chosen: 73, 110, 534 eV for Al, Ce and Au respectively. The so-called "three windows" technique was used for elemental mappings. Two images were taken, one below the edge and one on the edge. The edge background was determined by a power law method using the two pre-edge images and the edge background was subtracted to the image to obtain the true edge signal.

XPS spectra were collected on a SPECS (Phoibos MCD 150) X-ray photoelectron spectrometer, using a Mg Kα ($h\nu$ = 1253.6 eV) X-ray source having a 150 W (12 mA, 12.5 kV) electron beam power and a 7 mm × 20 mm spot size. The emission of photoelectrons from the sample was analyzed at a takeoff angle of 90° under ultra high vacuum conditions (1×10^{-8} Pa). XP spectra were collected at pass energy of 15 eV for C_{1s} and Au_{4f} core XPS levels. No charge compensation was applied during acquisition. After data collection, the binding energies were calibrated with respect to the binding energy of the C_{1s} peak at 284.8 eV [26]. The XPS measurements of the calcined samples were carried out at liquid nitrogen temperature to prevent gold reduction by X-rays or UHV and those of the reduced samples, at 25 °C. Spectrum processing was carried out using the Casa XPS software package and Origin 7.1 (Origin Lab Corporation).

2.3. Catalytic reactions

Catalytic reactions, i.e., CO oxidation and propene oxidation were carried out in a flow-type packed bed reactor with 50 and 150 mg of catalyst respectively, after *in situ* activation in 9 vol.% O_2 in He at 500 °C (calcination) or H_2 at 300 °C (reduction) (100 mL min^{-1}, 2 °C min^{-1} from room temperature to the final temperature, then 2 h at the final temperature). Catalyst bed temperature was controlled through an electronic controller.

CO oxidation was performed at room temperature, with the reactor immersed in a water bath, and atmospheric pressure with a feed of 1% CO, 9% O_2 and He (total flow rate 230 mL min^{-1}). CO consumption and CO_2 production were monitored simultaneously with a Maihak Gas IR Analyzer S710. Activities were measured after 20 min of reaction.

Table 1
Elemental analyses, $T_{50\%}$ in propene oxidation, gold particle sizes, and CO oxidation activity for the calcined and reduced catalysts.

Catalyst	Elemental analysis (wt%)		$S_{B.E.T.}$ ($m^2 g^{-1}$)	Propene oxidation $T_{50\%}$ (°C)		Gold particle size (nm)		CO oxidation activity at RT[b] ($\times 10^4 mol_{CO} s^{-1} g_{Au}^{-1}$)	
	Au	CeO_2		Calcination	Reduction	Calcination	Reduction	Calcination	Reduction
Au/Al_2O_3	0.88	–	110	360	340	2.4 (0.56)[a]	2.0 (0.49)	0	0
$Au/1.5CeO_2$-Al_2O_3	0.93	1.41	105	235	232	2.6 (0.55)	2.3 (0.52)	2.4	3.1
$Au/3CeO_2$-Al_2O_3	0.99	2.64	102	240	229	2.7 (0.53)	2.3 (0.45)	2.1	4.0
$Au/5CeO_2$-Al_2O_3	0.89	4.26	99	250	225	2.6 (0.43)	2.2 (0.47)	1.9	4.7
$Au/10CeO_2$-Al_2O_3	0.89	8.06	92	265	215	2.6 (0.57)	2.0 (0.45)	1.7	8.9
Au/CeO_2	0.97	98.3	200	175	165	n.m.	n.m.	0	9.9

n.m.: not measurable.
[a] Standard deviation.
[b] Activity measured at steady-state.

For propene oxidation, the reactant concentrations were 1200 ppm C_3H_6 and 9 vol.% O_2 in He (total gas flow rate of 150 mL min^{-1}). The reaction temperature was increased stepwise from room temperature to 300 °C at a heating rate of 1 °C min^{-1} with 1 h temperature plateau every 25 or 50 °C. The heating rate was purposefully chosen low in order to limit the exothermal effect of the reaction. Moreover, the activity at each temperature was measured after stabilization of the CO_2 production monitored in real time with an IR detector (ADC). After about 10 min at the temperature plateau, the CO_2 production became stable after an initial decrease, and after 30–40 min, the GC analysis was performed. No deactivation was observed during the measurement at each plateau of temperature (1 h). The analysis of propene and products other that CO and CO_2 was performed by gas chromatograph (Perichrom PR1525 equipped with a Varian WSCOT fused silica column (50 m × 0.32 mm id). The reproducibility of the catalytic results was checked for all the catalysts. The variation in the $T_{50\%}$ during the reproducibility tests was negligible (less than 2 °C).

3. Results

3.1. Characterization: BET, XRD, chemical analysis and sample color

Pure Al_2O_3 support initially had a BET surface area of 110 $m^2 g^{-1}$, which slightly decreases as the CeO_2 loading increases: 105, 102, 99 and 92 $m^2 g^{-1}$ for 1.5, 3, 5 and 10 wt% CeO_2 loading, respectively. The amounts of CeO_2 in $xCeO_2$-Al_2O_3 supports determined by elemental analysis are close to the theoretical loadings (Table 1).

The gold loadings of the catalysts are also close to the nominal loading of 1 wt% (Table 1), showing the effectiveness of the DPU preparation method on CeO_2-Al_2O_3 supports.

The color of the gold samples depends upon ceria loading and catalyst pre-treatment, and is a good indicator of the overall gold oxidation state [22]. The yellow color of as prepared Au/CeO_2 does not change after calcination at 500 °C. This means that gold was not reduced during calcination at 500 °C, in agreement with former reports [13,22]. In contrast, the color of Au/Al_2O_3 changes from pale yellow to violet, indicating the presence of Au^0. After reduction at 300 °C, Au/CeO_2 is dark brown and Au/Al_2O_3, red brown, and according to former characterizations [22], gold is fully reduced. The color of all the $Au/xCeO_2$-Al_2O_3 samples changes from yellow to grayish-violet after calcination, without significant difference in color between the different samples, and to brownish-violet color after reduction. These observations indicate the presence of Au^0 in the samples after both types of activation treatment. The difference of color between reduced and calcined samples may be due to the fact that that the whole gold is not reduced in the calcined samples or that the gold particle size is slightly different.

Fig. 1 reports the XRD profiles of the calcined CeO_2-Al_2O_3 samples. The XRD profile of the $1.5CeO_2$-Al_2O_3 sample (b) is similar to that of bare alumina (a) whereas for higher ceria loadings, diffraction peaks pertaining to CeO_2 appear and increase in intensity with the ceria loading. For the $10CeO_2$-Al_2O_3 sample (e), the broad diffraction lines due to CeO_2 (PDF-ICDD 34-0394) correspond to an average crystallite size of 8 nm (based on the Scherrer formula applied to peak (1 1 1) at $2\theta = 28.6°$). Assuming an ideal fluorite-type ceria lattice with a cell parameter of 0.5411 nm, one can calculate that the theoretical ceria loading corresponding to one monolayer coverage on the alumina of 110 $m^2 g^{-1}$ we used, is 10.7 wt%. Assuming that the ceria particles are hemispherical and 8 nm size in average and that the ceria density is 7.3 g cm^{-3}, one can calculate that the surface of alumina covered by CeO_2 in $10CeO_2$-Al_2O_3, is 5.1 $m^2 g^{-1}$. The alumina surface (110 $m^2 g^{-1}$) is therefore far from fully covered by ceria.

A close examination of the TEM images in high resolution of the various supports (figure not shown) allowed us to see particles on the $5CeO_2$-Al_2O_3 and $10CeO_2$-Al_2O_3 that could be attributed to 3D-CeO_2 particles. This was deduced from the measurement of the interplanar distance of 3.0 Å, which was consistent with the (1 1 1) distance of cerium oxide. No such particles could be observed in the TEM images of the $1.5CeO_2$-Al_2O_3 and $3CeO_2$-Al_2O_3 samples.

According to Martinez-Arias et al. [16], there are two main types of ceria species in $xCeO_2$-Al_2O_3 (x = 1, 2, 10 and 39%) prepared by impregnation then calcination: two-dimensional patches (2D-CeO_2) and crystallized ceria particles (3D-CeO_2). The relative amounts of each of these species do not linearly vary with the cerium loading: as the cerium content increased, the amount of 3D-CeO_2 gradually increases whereas the amount of 2D-CeO_2 initially increases up to 10 wt% CeO_2, then decreases. From our XRD and TEM results and the Martinez-Arias's results, it is proposed

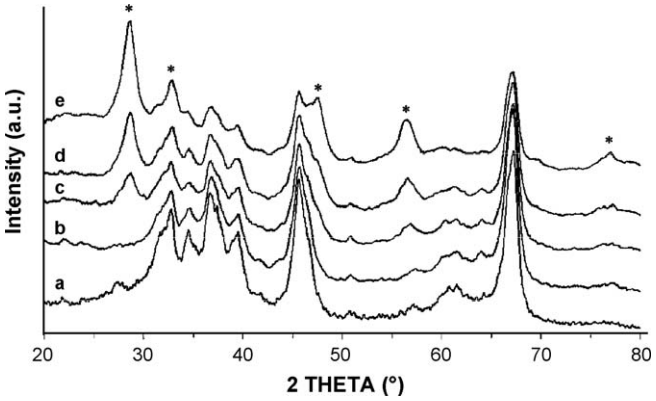

Fig. 1. XRD profile of Al_2O_3 and CeO_2-Al_2O_3 samples with different loadings of CeO_2 (*lines due to CeO_2): (a) Al_2O_3; (b) $1.5CeO_2$-Al_2O_3; (c) $3CeO_2$-Al_2O_3; (d) $5CeO_2$-Al_2O_3; (e) $10CeO_2$-Al_2O_3.

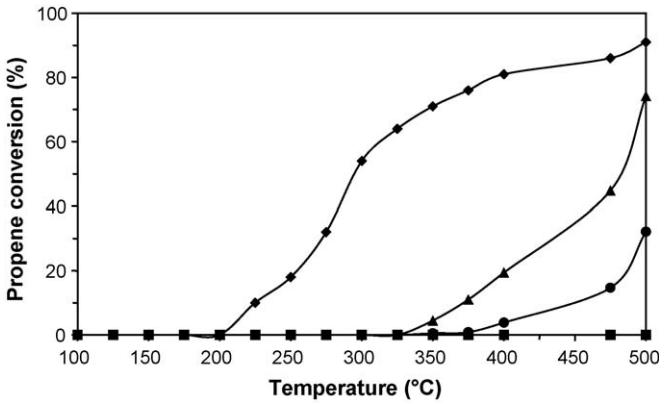

Fig. 2. Catalytic activity in propene oxidation of calcined pure supports as a function of the temperature: (■) Al_2O_3; (◆) CeO_2; (●) 1.5CeO_2-Al_2O_3; (▲) 10CeO_2-Al_2O_3.

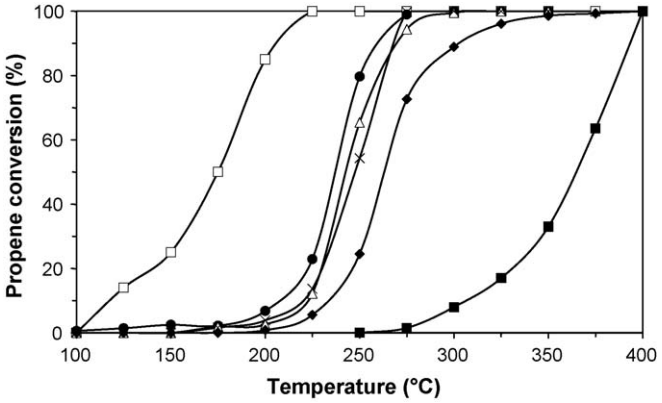

Fig. 4. Catalytic activity in propene oxidation of calcined samples as a function of the temperature: (□) Au/CeO_2; (●) Au/1.5CeO_2-Al_2O_3; (▲) Au/3CeO_2-Al_2O_3; (⋇) Au/5CeO_2-Al_2O_3; (◆) Au/10CeO_2-Al_2O_3; (■) Au/Al_2O_3.

that up to 3 wt% CeO_2, ceria mainly forms two-dimensional patches, and that above this loading, it also forms 3D-nanoparticles. Note that the XRD profiles do not exhibit diffraction peaks of gold in the Au/$x$$CeO_2$-$Al_2O_3$ samples, whether they are calcined or reduced.

3.2. Propene oxidation

Propene conversion and CO_2 evolution were measured simultaneously during the catalytic reaction, and it was observed that propene was 100% converted into CO_2 at any temperature; thus all the samples are 100% selective. The pure oxide supports, CeO_2, Al_2O_3, 1.5CeO_2-Al_2O_3, and 10CeO_2-Al_2O_3, were first tested (Fig. 2). Pure Al_2O_3 is totally inactive in contrast with CeO_2, which is active with a light-off temperature, $T_{50\%}$ of 300 °C. CeO_2 on alumina exhibits an intermediate activity that increases with the ceria loading.

When gold is present, and the samples are activated under H_2 (Fig. 3), Au/Al_2O_3 becomes active ($T_{50\%}$ = 340 °C) (Table 1), but it still exhibits the lowest catalytic activity while Au/CeO_2 is the most active catalyst ($T_{50\%}$ = 165 °C). The reduced Au/$x$$CeO_2$-$Al_2O_3$ samples exhibited intermediate activities. Interestingly, the addition of a very small quantity of CeO_2 (1.5 wt%) to Al_2O_3 induces a drastic low temperature shift of the light-off temperature from 340 °C for Au/Al_2O_3 to 232 °C, i.e., an increase of activity. Further increase in ceria loadings to 3, 5 and 10 wt% leads to further decrease of the $T_{50\%}$ to 229, 225, and 215 °C, respectively (Table 1).

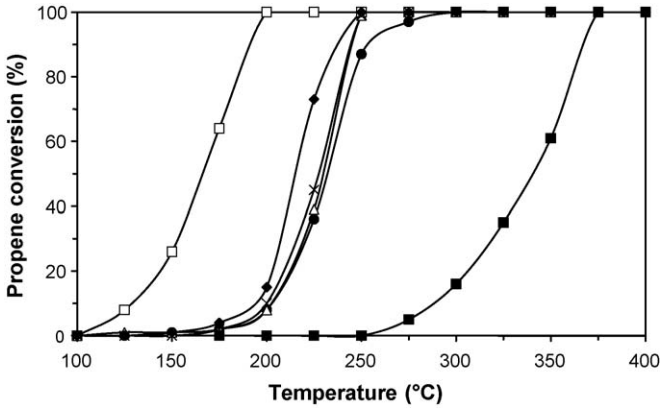

Fig. 3. Catalytic activity in propene oxidation of reduced samples as a function of the temperature: (□) Au/CeO_2; (●) Au/1.5CeO_2-Al_2O_3; (▲) Au/3CeO_2-Al_2O_3; (⋇) Au/5CeO_2-Al_2O_3; (◆) Au/10CeO_2-Al_2O_3; (■) Au/Al_2O_3.

Note that this decrease is small but significant; we could observe it on repeated experiments. Hence, the catalytic activity of the reduced samples increases as the ceria loading increases from 1.5 to 10 wt%.

Fig. 4 gathers the catalytic activity of the gold samples calcined under O_2 in He. At the first glance, Fig. 4 looks similar to Fig. 3; again the Au/$x$$CeO_2$-$Al_2O_3$ catalysts are less active than Au/CeO_2

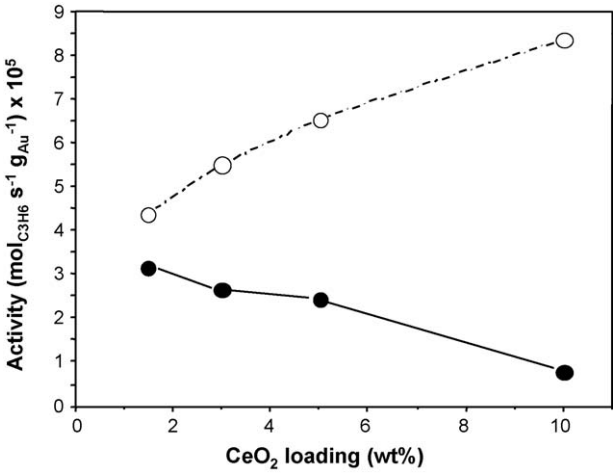

Fig. 5. Variation of the activity in propene oxidation measured at 235 °C as a function of the CeO_2 loading for calcined ((●) solid line) and reduced samples ((○) dotted line).

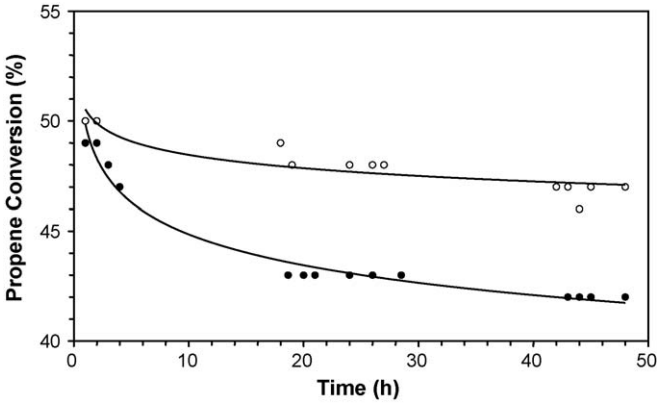

Fig. 6. Evolution of the propene conversion with time on stream for reduced catalysts Au/CeO_2 at 165 °C (●) and Au/10CeO_2-Al_2O_3 at 215 °C (○).

and more active than Au/Al_2O_3. However, first the activity of the calcined samples is lower than that of the reduced counterparts; the light-off temperatures are significantly higher (Table 1); second, the activity of the calcined $Au/xCeO_2$-Al_2O_3 samples decreases when the ceria loading increases. In other words, the reduced $Au/10CeO_2$-Al_2O_3 catalyst containing the highest amount of ceria, is the most active of the series, whereas after calcination, it is the least active sample, and *vice versa*. This difference between calcined and reduced samples also exists for the Au/Al_2O_3 and Au/CeO_2 catalysts but to a lesser extent. Fig. 5, which reports the activity measured at 235 °C for the two sets of $Au/xCeO_2/Al_2O_3$ samples, shows that at low ceria loading, the catalyst pre-treatment has a weak influence on the activity whereas as the ceria loading increases, the activation pre-treatment has a stronger effect, and the difference of activity increases. In order to interpret these results, the samples were characterized more extensively.

The stabilities of the Au/CeO_2-Al_2O_3 and Au/CeO_2 catalysts during time on stream were also compared. Fig. 6 compares the ones of $Au/10\%CeO_2$-Al_2O_3 and Au/CeO_2 at temperatures corresponding to 50% conversion, i.e., at 215 and 165 °C, respectively. It shows that $Au/10\%CeO_2/Al_2O_3$ exhibits better stability than Au/CeO_2 in spite of the higher reaction temperature. Hence, the use of alumina seems to lead to a beneficial effect in terms of stability.

3.3. Combined TEM-EFTEM characterization

Fig. 7b, d and f show the EFTEM micrographs of the calcined $Au/1.5CeO_2$-Al_2O_3 and $Au/10CeO_2$-Al_2O_3 and of the reduced

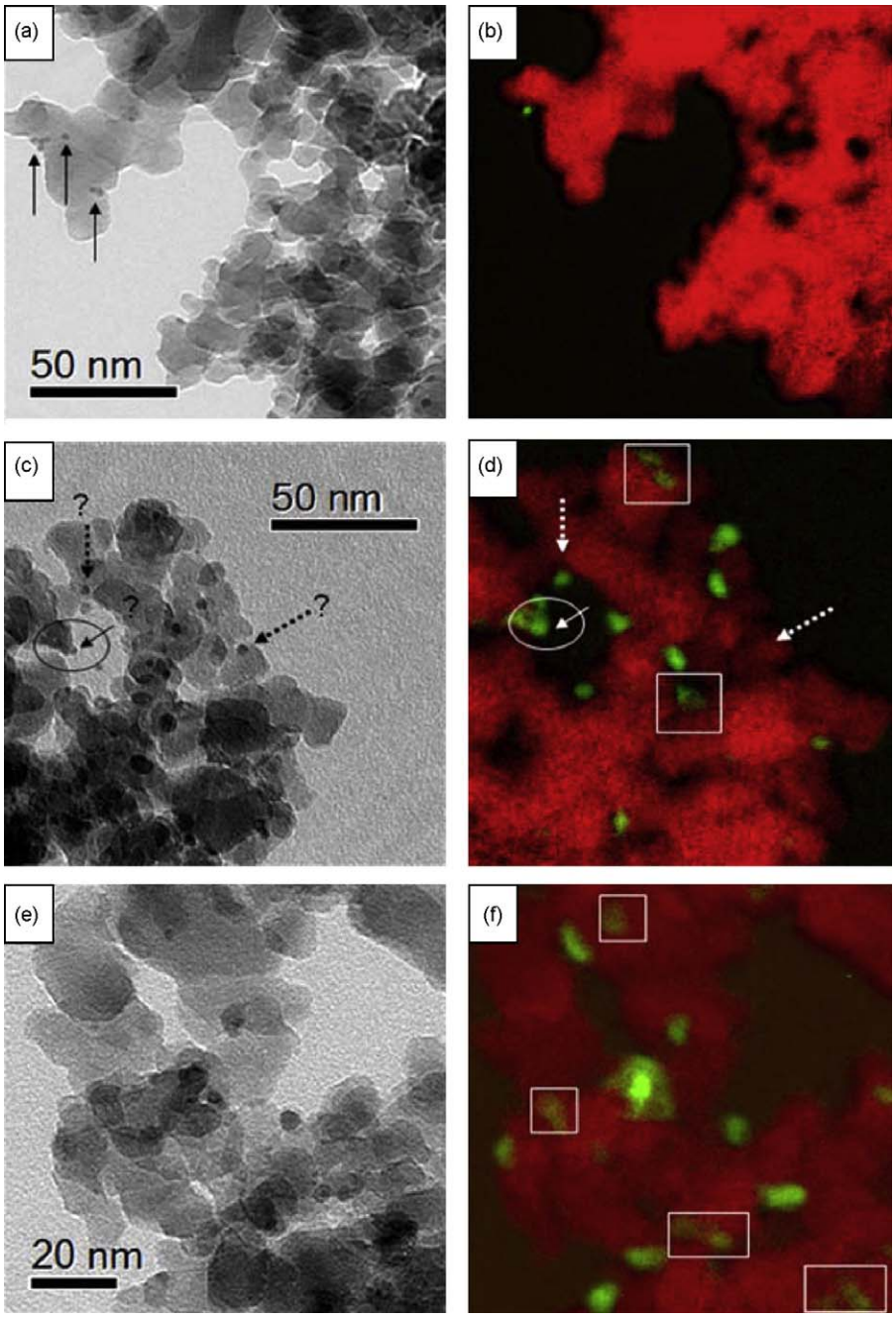

Fig. 7. Zero-loss TEM images and the corresponding EFTEM images : (a) and (b) calcined $Au/1.5CeO_2$-Al_2O_3; (c) and (d) calcined $Au/10CeO_2$-Al_2O_3; (e) and (f) reduced $Au/10CeO_2$-Al_2O_3.

$Au/10CeO_2$-Al_2O_3 samples. The EFTEM images show red areas corresponding to Al_2O_3, and green spots corresponding to ceria. The blue color expected for the gold element is not observed. This is due to the combination of two factors: the signal is weak because the gold particles are small (~2 nm) and the absorption edge for Au at 534 eV is a "saw-tooth"-type edge, thus the signal is intrinsically low. These images are accompanied by the corresponding zero-loss TEM micrographs, i.e., the plain TEM image (Fig. 7a, c and e).

For the calcined $Au/1.5CeO_2$-Al_2O_3 sample, small particles of ~2 nm are seen in the zero-loss TEM image indicated with arrows in Fig. 7a. Only one green spot indicating the presence of a ceria particle of ~2 nm (indicated with an arrow) is visible on the EFTEM image (Fig. 7b), but it is not visible on the TEM image (Fig. 7a). This allows the attribution of the small particles visible on the TEM image to gold particles. The quasi absence of signal corresponding to CeO_2 in the EFTEM image (Fig. 7b) is certainly due not only to the low amount of ceria in this sample, but also to the fact that at this loading, ceria is well dispersed as bi-dimensional particles or as isolated cations on the alumina support, and therefore cannot be detected.

The increase in ceria loading to 10 wt% results into drastic changes in the EFTEM image. Bright green spots of CeO_2 are now clearly visible both for the calcined (Fig. 7d) and reduced sample (Fig. 7f), and reveal the presence of 3-D CeO_2 particles of about 10 nm size, in agreement with the XRD results. The pale green spots, surrounded by squares in Fig. 7d, indicate CeO_2 particles, probably bi-dimensional; they seem more numerous than in $Au/1.5CeO_2$-Al_2O_3. The same type of image is observed with the reduced $Au/10CeO_2$-Al_2O_3 sample (Fig. 7f). Again, one can note that the ceria particles clearly visible on the EFTEM images are barely visible on the zero-loss image. Hence, thanks to the EFTEM technique, it is possible to rather unambiguously differentiate gold particles from ceria particles.

A question, which arises, is whether the gold nanoparticles are located on alumina or on ceria. Al and Ce mapping of $Au/xCeO_2$-Al_2O_3 samples can also provide this element of information. If one considers the three small gold particles marked with arrows in the zero-loss image of $Au/10CeO_2$-Al_2O_3 (Fig. 7c), two of them (dotted arrows) correspond to a red area in the EFTEM image (Fig. 7d), indicating that they are located on bare alumina or on alumina on which ceria is highly dispersed; the third one was found close to a green spot (full arrow), which may indicate that it interacts with a ceria particle. Note that this observation has been made possible only because of the side-on view gold particles on ceria.

3.4. TEM characterization

If XRD diffractograms do not reveal the presence of gold particles in the $Au/xCeO_2$-Al_2O_3 samples, the TEM images show small particles in all samples, except in Au/CeO_2, which can now be attributed to gold and not to ceria particles, based on the previous EFTEM analysis. Table 1 reports the gold particle sizes measured in all samples after calcination and reduction. For each set of samples, reduced and calcined, the gold particle size is roughly the same whatever the ceria loading, with similar average sizes and standard deviations. The particles are slightly smaller in the reduced samples (~2.2 nm) than in the calcined ones (~2.6 nm), and they are of the same size as for Au/Al_2O_3. As mentioned in Section 1, gold particles are not visible in reduced and calcined Au/CeO_2. Note however, that catalytic results of selective hydrogenation of butadiene led us to conclude that the gold particles were of the same size in reduced 1 wt% Au/Al_2O_3 and 1 wt% Au/CeO_2 [27]. Let us also remind that gold on ceria (1 wt%) is not reduced after calcination [22].

It must be stressed that during the analysis of the TEM images, we observed that the density of gold particles per surface unit of support decreases as the ceria loading increased, and that the density of gold particles seems to be roughly the same for the calcined and reduced samples. This can be seen in Fig. 8, which shows typical micrographs of $Au/1.5CeO_2$-Al_2O_3 and $Au/10CeO_2$-Al_2O_3 samples obtained after reduction and calcination. Since the average gold particle size does not depend on the ceria loading, and is quite constant, the decrease in particle density as the ceria loading increases is an indication that some particles are missing or cannot be observed. One can propose that a fraction of gold interacts with ceria on which the particles cannot be detected, and that the percentage of gold on ceria increases with the ceria loading. This interpretation needs to be confirmed, but it is in agreement with the fact that in an EFTEM image (Fig. 7d), one gold particle could be seen in interaction with a ceria particle. Moreover

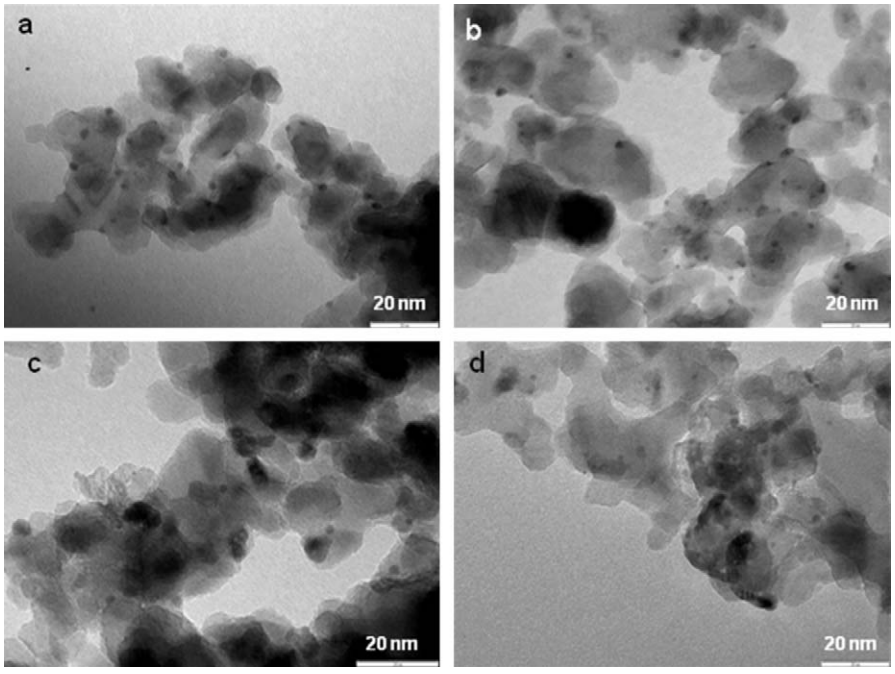

Fig. 8. TEM micrographs of $Au/1.5CeO_2$-Al_2O_3 (a—calcined, b—reduced) and $Au/10CeO_2$-Al_2O_3 sample (c—calcined, d—reduced).

some gold particles could be located on 2-D ceria particles that would be too thin to be detected by EFTEM.

3.5. XPS results

In order to determine the influence of the ceria loading on the gold oxidation state in reduced and calcined samples, XPS measurements were performed (Fig. 9). Note that the Au(4f) XP spectra of the reduced samples were measured at 25 °C whereas those of the calcined ceria-based samples were recorded at liquid nitrogen temperature, in order to prevent uncontrolled gold reduction by X-rays or UHV as much as possible.

The XP spectra of the reference samples, i.e., Au/Al_2O_3 and Au/CeO_2 were first compared. The spectra of reduced and calcined Au/Al_2O_3 (Fig. 9a and b) exhibit the same $Au(4f_{7/2})$ peak at 83.4 eV and $Au(4f_{5/2})$ peak at 87.1 eV, which is consistent with the binding energies of Au^0 [18,19]. Hence gold is fully reduced in these samples, in agreement with former works [8,22]. The spectrum of reduced Au/CeO_2 (Fig. 9c) looks similar to that of Au/Al_2O_3 although the peaks are slightly shifted (83.7 and 87.4 eV). The spectrum of the calcined Au/CeO_2 sample (Fig. 9d) is totally different since it shows peaks at higher binding energy. The analysis of this spectrum performed in a previous paper [8] showed that it can be decomposed into three contributions: 31% of Au^{III}, 50% of $Au^{\delta+}$ and 19% of Au^0, attesting for gold reduction during XPS measurement even performed at low temperature since gold was expected to remain as Au^{III} after calcination [22]. This makes quantitative evaluation of the percentages of the oxidation states impossible and interpretation complicated.

The spectra of the reduced $Au/1.5CeO_2$-Al_2O_3 (Fig. 9h) and $Au/10CeO_2$-Al_2O_3 samples (Fig. 9i) are similar to that of Au/Al_2O_3 (Fig. 9a and b), indicating that gold is fully reduced in these samples. The spectrum of calcined $Au/1.5CeO_2$-Al_2O_3 (Fig. 9e) also resembles to that of Au/Al_2O_3. However, as the ceria loading increases, i.e., for $Au/5CeO_2$-Al_2O_3 (Fig. 9f) and especially for $Au/10CeO_2$-Al_2O_3 samples (Fig. 9g), the maximum of the $Au4f_{7/2}$ peak is slightly shifted to higher binding energies compared to the reduced samples whose B.E. does not vary (Fig. 9h and i). This small shift might be considered as an indication that the average gold oxidation state slightly increases with the ceria loading in the calcined samples. This probably arises from the fraction of gold interacting with ceria, which increases with the CeO_2 loading and does not reduce during calcination as in the case of calcined Au/CeO_2. Reduction occurring during the XPS measurements may be responsible for the limited differences observed.

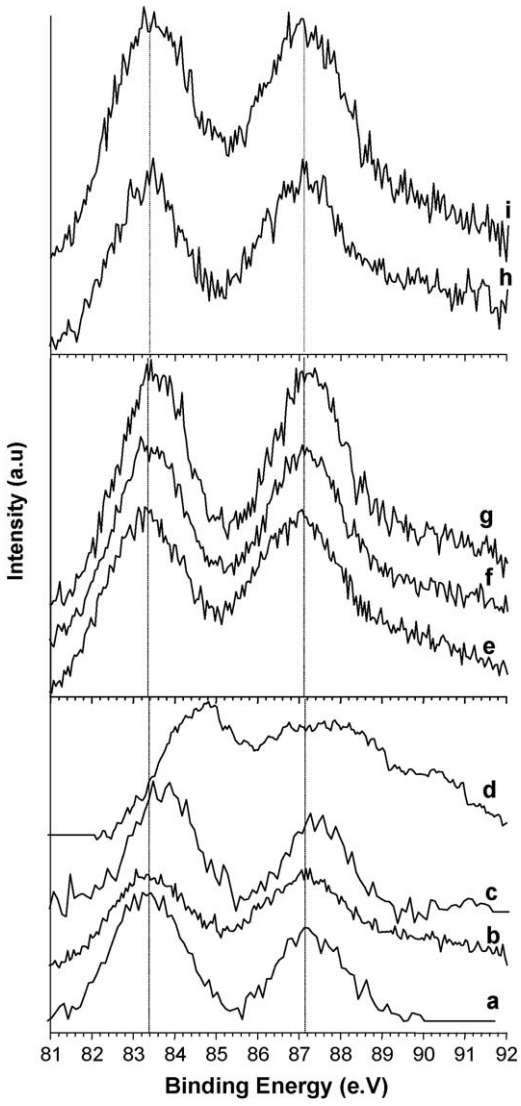

Fig. 9. Au(4f) XP spectra of (a) reduced Au/Al_2O_3; (b) calcined Au/Al_2O_3; (c) reduced Au/CeO_2; (d) calcined Au/CeO_2;(e) calcined $Au/1.5CeO_2$-Al_2O_3; (f) calcined $Au/5CeO_2$-Al_2O_3; (g) calcined $Au/10CeO_2$-Al_2O_3; (h) reduced $Au/1.5CeO_2$-Al_2O_3; (i) reduced $Au/10CeO_2$-Al_2O_3. The measurements of spectra (b), (d), (e), (f), and (g) were performed at 100 K, and the other spectra at room temperature.

3.6. CO oxidation reaction

In order to obtain further information on the presence of oxidized or metallic gold in the calcined and reduced $Au/xCeO_2$-Al_2O_3 samples, the reaction of CO oxidation was performed at room temperature over these catalysts. In agreement with our former work [22], Au/Al_2O_3 is inactive (Table 1) in spite of the presence of Au^0 because non-reducible support leads to inactive catalysts. Calcined Au/CeO_2 is also inactive because of the absence of Au^0. Indirectly, this result confirms that gold in calcined Au/CeO_2 was partially reduced during XPS measurement (Fig. 9d).

The pure $xCeO_2/Al_2O_3$ supports are inactive whereas all the $Au/xCeO_2$-Al_2O_3 samples show an activity in CO oxidation at room temperature (Table 1), intermediate between that of Au/CeO_2 and Au/Al_2O_3 in the case of the reduced samples, indicating the presence of Au^0 interacting with ceria whether the samples are calcined or reduced. The calcined samples are less active than the reduced ones. Moreover, for the reduced $Au/xCeO_2$-Al_2O_3 samples, the activity increases from 3.0 to 8.9 $\times 10^{-4}$ mol_{CO} s^{-1} $g_{Au}{}^{-1}$ as the ceria loading increases from 1.5 to 10% (Fig. 10, dotted line). This

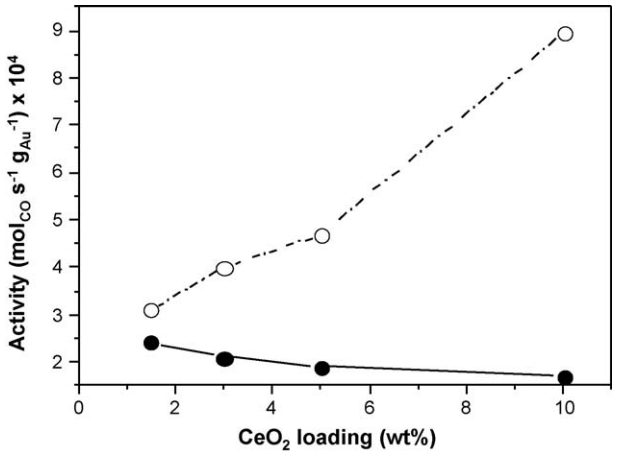

Fig. 10. Variation of the activity in CO oxidation measured at RT as a function of the CeO_2 loading for calcined ((●) solid line) and reduced samples ((○) dotted line).

result is consistent with the TEM results, i.e., the gold particle size is constant, but there is an increasing fraction of gold interacting with ceria when the ceria loading increases. In contrast for the calcined samples, the activity decreases from 2.4 to 1.6×10^{-4} mol_{CO} s^{-1} $g_{Au}{}^{-1}$ as the ceria loading increases (Fig. 10, solid line). This may be due to the fact that as the fraction of gold interacting with ceria increases when the ceria loading increases, the fraction of unreduced gold species, inactive in CO oxidation, increases.

4. Discussion

The catalytic results show that the addition of small amounts of ceria on alumina (1.5–10 wt% CeO_2) has a drastic effect on the catalytic activity in propene oxidation of the gold catalysts since the activity is found "intermediate" between that of Au/CeO_2 and Au/Al_2O_3 whether the samples have been activated under hydrogen or oxygen (Figs. 3 and 4). The fact that the $Au/xCeO_2$-Al_2O_3 catalysts are more active than Au/Al_2O_3 can be interpreted by the fact that part of the gold interacts with ceria. This assumption is consistent with the observation by TEM that the density of gold particles (visible only on alumina) decreases when the ceria loading increases and by EFTEM that the amount of metallic gold interacting with ceria increases.

A close examination of the catalytic results (Table 1 and Fig. 5) shows that all the calcined samples (Au/CeO_2, Au/Al_2O_3 and $Au/xCeO_2/Al_2O_3$) are less active in propene oxidation than the reduced ones. The difference could be first attributed to the difference in the average gold particle size, which is slightly larger in the calcined samples than in the reduced ones (Table 1). The case of $Au/xCeO_2$-Al_2O_3 catalysts is intricate since the difference in propene oxidation activity between the calcined and reduced samples increases with the ceria loading while the gold particle size does not drastically change (Fig. 5 and Table 1).

If one considers first the reduced $Au/xCeO_2$-Al_2O_3 samples, the catalyst activity increases with ceria loading. Their pink-brown color, XPS gold binding energies and activity in CO oxidation attest that these samples mainly contain metallic gold. Moreover, the increase in activity in CO oxidation with ceria loading confirms the results of electron microscopy that there is an increasing amount of metallic gold interacting with ceria as the ceria loading increases. The increasing activity in propene oxidation with the ceria loading is consistent with the fact that gold on ceria is more active than gold on alumina.

The decreasing activity of the calcined $Au/xCeO_2$-Al_2O_3 samples, in propene oxidation and CO oxidation, as the ceria loading increases can also be interpreted by the fact that the percentage of gold on ceria increases with the ceria loading. The capacity of ceria-based supports to prevent extensive reduction of cationic gold species under oxidative treatment has already been reported in the literature, especially when nanosized ceria is used [28–31] and we have previously reported that gold in 1 wt% Au/CeO_2 is not reduced upon calcination at 500 °C [22]. Even though the $Au/10CeO_2$-Al_2O_3 catalyst contains less ceria than the theoretical monolayer coverage (10.7 wt%), EFTEM analyses reveal that CeO_2 was present as dispersed species in the form of two-dimensional patches (2D-CeO_2) and also as aggregated crystalline species (3D-CeO_2 particles of ~10 nm size) (Fig. 9). These 3D-CeO_2 particles are expected to favor the stabilization of part of gold under an oxidized state during calcination. This assumption is supported by the slight shift to higher energy of the Au XP spectra observed as the ceria loading increases (Fig. 9e–g), which is an indication that the overall gold oxidation state slightly increases with the ceria loading. Based on our previous works [8,22], unreduced gold is not active species in CO and propene oxidation, both of which require the presence of metallic gold. Note that gold in calcined Au/CeO_2 becomes active in propene oxidation because it reduces during the reaction [8]. However, since the calcined $Au/xCeO_2$-Al_2O_3 samples show an activity in CO oxidation whatever the ceria content, some metallic gold must be in interaction with the ceria particles supported on the surface of alumina. It is also possible that gold nanoparticles supported on alumina at the vicinity of the CeO_2 aggregates are responsible for this activity or that part of the gold interacting with two-dimensional patches of CeO_2 is reduced, and is therefore active.

For the calcined $Au/xCeO_2$-Al_2O_3 catalysts, it may be concluded that the decreasing activity in CO and propene oxidation when the ceria loading increases, is due to an increasing fraction of gold interacting with ceria, part of it remaining unreduced. There are reports in the literature for the deviation from zero towards higher oxidation states in Pt or Pd supported on $xCeO_2$-Al_2O_3 as the ceria loading increases. In the case of $Pt/xCeO_2$-Al_2O_3 catalysts (1 wt% Pt, x = 0.5, 1, 3, 6 and 10 wt% CeO_2 on Al_2O_3, calcined at 500 °C in air) [32], this was deduced from the shift of the XPS Pt(4d) binding energy from 315.0 to 315.6 and 315.8 eV, as ceria loading increased from 3 to 6 and 12 wt%, respectively. In the case of $Pd/xCeO_2$-Al_2O_3 catalysts (1 wt% Pd, x = 6, 11 and 19 wt%, calcined at 500 °C in air) [33], this was deduced from the calculation of the hydrogen consumed during TPR, due to the reduction of PdO [33].

5. Conclusion

The influence of the ceria loading (1.5–10 wt% CeO_2) and of the activation conditions (calcination or reduction) of $Au/xCeO_2$-Al_2O_3 catalysts on the catalytic properties for total oxidation of propene under excess oxygen was examined. The presence of ceria, even in low amount, strongly enhanced the catalytic activity compared to gold on mere alumina. The catalysts are less active than gold on pure ceria, but there are more stable during time on stream. Depending on the ceria loading, ceria was found to be present as 3-D nanoparticles and/or 2-D patches on alumina. TEM analyses showed that the density of visible gold nanoparticles, i.e., those located on alumina, decreased when the ceria loading increased, indicating that gold also interacts with the ceria particles; EFTEM indeed revealed that some gold particles were in close contact with CeO_2 particles. The XPS data and the catalytic results of CO oxidation showed that the nature of the activation treatment influenced the oxidation state of gold. In the reduced $Au/xCeO_2$-Al_2O_3 samples, all gold was metallic whereas in the calcined ones, in addition to Au^0 on alumina, there was an increasing amount of unreduced gold as the ceria loading increased. Reduced samples were found more active than calcined samples in propene oxidation. Moreover, the activity of the reduced samples increased with the ceria loading whereas it decreased for the calcined samples. These differences are due to the fact that metallic gold is more active than oxidized gold and Au^0 on ceria is more active than Au^0 on alumina. The capacity of ceria to stabilize gold in an oxidized state was considered as the main parameter responsible for the difference of activity in propene oxidation between the calcined and reduced $Au/xCeO_2$-Al_2O_3 catalysts. The ceria content, i.e., the proportion of gold interacting with ceria, and the activation procedure, i.e., the oxidation state of gold, both influence the catalytic activity.

Acknowledgement

The authors acknowledge the ANR (Agence Nationale pour la Recherche), which sponsored this work (ANR-BLANC07-2 183612).

References

[1] G.C. Bond, C. Louis, D.T. Thompson, Catalysis by Gold, ICP press, 2006.
[2] S. Scirè, S. Minico, C. Crisafulli, C. Satriano, A. Pistone, Appl. Catal. B 40 (2003) 43.

[3] C.D. Pina, N. Dimitratos, E. Falletta, M. Rossi, A. Siani, Gold Bull. 40 (2007) 67.
[4] A.C. Gluhoi, N. Bogdanchikova, B.E. Nieuwenhuys, J. Catal. 229 (2005) 154.
[5] X. Yang, Y. Shen, L. Bao, H. Zhu, Z. Yuan, React. Kinet. Catal. Lett. 93 (2008) 19.
[6] S.Y. Liu, S.M. Yang, Appl. Catal. A 334 (2008) 92.
[7] R. Nedyalkova, L. Ilieva, M.C. Bernard, A. Hugot-Le Goff, D. Andreeva, Mater. Chem. Phys. 116 (2009) 214.
[8] L. Delannoy, K. Fajerwerg, P. Lakshmanan, C. Potvin, C. Méthivier, C. Louis, Appl. Catal. B 94 (2010) 117–124.
[9] G.C. Bond, D.T. Thompson, Catal. Rev. Sci. Eng. 41 (1999) 319.
[10] Z.R. Tang, J.K. Edwards, J.K. Bartley, S.H. Taylor, A.F. Carley, A.A. Herzing, C.J. Kiely, G.J. Hutchings, J. Catal. 249 (2007) 208.
[11] F. Moreau, G.C. Bond, Catal. Today 122 (2007) 215.
[12] A. Karpenko, R. Leppelt, V. Plzak, J. Cai, A. Chuvilin, B. Schumacher, U. Kaiser, R.J. Behm, Top. Catal. 44 (2007) 183.
[13] R. Si, M.F. Stephanopoulos, Angew. Chem. Int. Ed. 47 (2008) 2884.
[14] A. Trovarelli, Catal. Rev. Sci. Eng. 38 (1996) 439.
[15] A. Piras, A. Trovarelli, G. Dolcetti, Appl. Catal. B 28 (2000) L77.
[16] A. Martínez-Arias, M. Fernández-García, L.N. Salamanca, R.X. Valenzuela, J.C. Conesa, J. Soria, J. Phys. Chem. B 104 (2000) 4038.
[17] J.J. Spivey, Ind. Eng. Chem. Res. 26 (1987) 2165.
[18] M.A. Centeno, M. Paulis, M. Montes, J.A. Odriozola, Appl. Catal. A 234 (2002) 65.
[19] L. Ilieva, G. Pantaleo, J.W. Sobczak, I. Ivanov, A.M. Venezia, D. Andreeva, Appl. Catal. B 76 (2007) 107.
[20] R. Zanella, S. Giorgio, C.R. Henry, C. Louis, J. Phys. Chem. B 106 (2002) 7634.
[21] R. Zanella, L. Delannoy, C. Louis, Appl. Catal. A 291 (2005) 62.
[22] L. Delannoy, N. Weiher, N. Tsapatsaris, A.M. Beesley, L. Nchari, S.L.M. Schroeder, C. Louis, Top. Catal. 44 (2007) 263.
[23] T. Akita, M. Okumura, K. Tanaka, M. Kohyama, M. Haruta, J. Mater. Sci. 40 (2005) 3101.
[24] T. Akita, K. Tanaka, M. Kohyama, M. Haruta, Catal. Today 122 (2007) 233.
[25] R. Zanella, C. Louis, Catal. Today 107 (2005) 768.
[26] T.L. Barr, S. Seal, L.M. Chen, C.C. Kao, Thin Solid Films 253 (1994) 277.
[27] A. Hugon, L. Delannoy, C. Louis, Gold Bull. 41 (2008) 127.
[28] S. Carrettin, A. Corma, M. Iglesias, F. Sanchez, Appl. Catal. A 291 (2005) 247.
[29] P. Concepcion, S. Carrettin, A. Corma, Appl. Catal. A 307 (2006) 42.
[30] W. Deng, A.I. Frenkel, R. Si, M. Flytzani-Stephanopoulos, J. Phys. Chem. C 112 (2008) 12834.
[31] F. Vindigni, M. Manzoli, A. Chiorino, T. Tabakova, F. Boccuzzi, J. Phys. Chem. B 110 (2006) 23329.
[32] S. Damyanova, J.M.C. Bueno, Appl. Catal. A 253 (2003) 135.
[33] L.S.F. Feio, C.E. Hori, L.V. Mattos, D. Zanchet, F.B. Noronha, J.M.C. Bueno, Appl. Catal. A 348 (2008) 183.